Multi-Sinusoidal Waveform Shaping for Integrated Data and Energy Transfer in Aging Channels

Jie Hu[1,2], Yaping Hou[1,2], Kun Yang[2,*]

[1] Yangtze Delta Region Institute (Huzhou), University of Electronic Science and Technology of China, Huzhou 313001, China

[2] School of Information and Communication Engineering, University of Electronic Science and Technology of China, Chengdu 611731, China

[*] The corresponding author, email: kunyang@uestc.edu.cn

Abstract: Integrated data and energy transfer (IDET) is capable of simultaneously delivering on-demand data and energy to low-power Internet of Everything (IoE) devices. We propose a multi-carrier IDET transceiver relying on superposition waveforms consisting of multi-sinusoidal signals for wireless energy transfer (WET) and orthogonal-frequency-division-multiplexing (OFDM) signals for wireless data transfer (WDT). The outdated channel state information (CSI) in aging channels is employed by the transmitter to shape IDET waveforms. With the constraints of transmission power and WDT requirement, the amplitudes and phases of the IDET waveform at the transmitter and the power splitter at the receiver are jointly optimised for maximising the average direct-current (DC) among a limited number of transmission frames with the existence of carrier-frequency-offset (CFO). For the amplitude optimisation, the original non-convex problem can be transformed into a reversed geometric programming problem, then it can be effectively solved with existing tools. As for the phase optimisation, the artificial bee colony (ABC) algorithm is invoked in order to deal with the non-convexity. Iteration between the amplitude optimisation and phase optimisation yields our joint design. Numerical results demonstrate the advantage of our joint design for the IDET waveform shaping with the existence of the CFO and the outdated CSI.

Keywords: integrated data and energy transfer (IDET); wireless energy transfer (WET); simultaneous wireless information and power transfer (SWIPT); carrier-frequency-offset (CFO); waveform; aging channels; outdated channel state information (CSI); orthogonal frequency division multiplexing (OFDM)

I. INTRODUCTION

In the era of Internet of Everything (IoE), IoE devices are massively deployed for environment monitoring and data processing. Due to frequent operations, the batteries of the IoE devices can be drained within a short time. Harvesting energy from radio-frequency (RF) signals has been envisioned as an effective way for energy supply [1, 2]. Relying on RF signals, integrated data and energy transfer (IDET) technique can provide flexible wireless energy transfer (WET) services, while satisfying the quality of service (QoS) of wireless data transfer (WDT) [3, 4]. However, traditional WDT waveforms have diverse amplitudes for modulating information, which results in unstable WET performance. Therefore, novel waveforms for conveying IDET services should be carefully investigated.

By exploiting multiple transmit antennas, IDET waveforms can be designed in the spatial domain for improving the performance [5–8]. Specifically, Yue *et al.* [5] designed a hybrid multicast beam with/without perfect channel-state-information (CSI) for IDET towards multiple data and energy users. Moreover, a robust beamforming design with channel estimation errors was studied in order to minimise the transmit power of a base-station delivering IDET services, while satisfying requirements of both data and energy users [6]. In [7], Zhao *et al.* proposed three transmission schemes based on receive spatial modulation aided IDET system with finite alphabet. Furthermore, Pan *et al.* [8] firstly introduced an intelligent reflecting surface (IRS) to assist IDET, since incident waveforms towards the IRS can be adjusted to benefit from additional spatial gains.

Coding and modulation can be relied upon for adjusting waveforms for IDET [9–13]. The first design guide for a coding and modulation controlled IDET system was proposed in [9]. Specifically, Zhao *et al.* [10] proposed a unary coding based IDET encoder by considering a practical M-QAM. In [11], the codeword distribution in a unary encoder was designed to maximise the WET performance with the required WDT constraint. Moreover, according to [9], different modulation schemes have diverse IDET performance. Therefore, an adaptive modulation based IDET transceiver was firstly investigated in [12], which significantly increased the attainable rate-energy region. In [13], the non-orthogonal multiple access (NOMA) technique was adopted by a transmitter by superimposing the modulated symbols destined to multiple WDT requesters in the power-domain. Then an energy interleaver and a constellation rotation-based modulator were jointly designed for maximising the attainable WET performance without any degradation of the WDT performance.

Since multi-sinusoidal (multi-tone) waveforms were widely regarded as an efficient way for WET [14], some of the existing works tried to modulate information by exploiting characteristics of these waveforms in order to deliver IDET services [15–17]. Specifically, Kim *et al.* [15] originally proposed a scheme of modulating information by exploiting different peak-to-average-power-ratio (PAPR) of multi-sinusoidal waveforms for delivering IDET services. Krikidis *et al.* [16] then proposed a tone-index of multi-sinusoidal waveforms based modulation (TIM) scheme for IDET. Furthermore, a multi-tone amplitude modulation (MAM) scheme modulates information on both the number of sinusoidal waveforms with different frequencies and on their amplitudes [17].

Furthermore, an orthogonal-frequency-division-multiplexing (OFDM) waveform for WDT [18, 19] is a special type of multi-sinusoidal waveforms with varying amplitudes and phases in its components. Therefore, careful designs on multi-sinusoidal waveforms for IDET have attracted a lot of attentions [20–24]. Specifically, Buckley [20] superimposed the unmodulated multicarrier signal onto the OFDM signal to improve the WET performance. By varying amplitudes and phases of the superimposed IDET waveform, the WET performance was maximised while satisfying the WDT performance constraint. Moreover, in [21], Kim proposed a realistic IDET system and demonstrated the benefit of jointly designing the OFDM waveform and the multi-sinusoidal waveforms. Buckley *et al.* [22] analysed the structure of OFDM waveform and they exploited cyclic prefix for dedicated WET, which effectively improved the overall IDET performance. In [23], a DC-filter is invoked at the receiver to filter the deterministic WET signals from the superposition signals so as to minimise the intra-subcarrier-interference. In [24], a joint subcarrier allocation and amplitude adjustment problem was formulated to minimise the outage of WDT in an OFDM assisted IDET system.

However, the drawbacks of above-mentioned works [20–24] can be summarized as follows:

- Perfect carrier frequency synchronization is assumed for IDET waveform design. However, it is not practical in low-power IoE devices with limited signal processing capabilities. The carrier-frequency-offset (CFO) caused by either the oscillator mismatch between the transmitter and the receiver or the Doppler shift can severely degrade the system performance, since it sabotages the orthogonality among subcarrier [25]. It is common to consider CFO for performance analysis in an OFDM based system [26].

- Their waveform design requires perfect CSI acquisition in every transmission frames. As a result, numerous energy and communication resources are consumed for CSI acquisition. It is

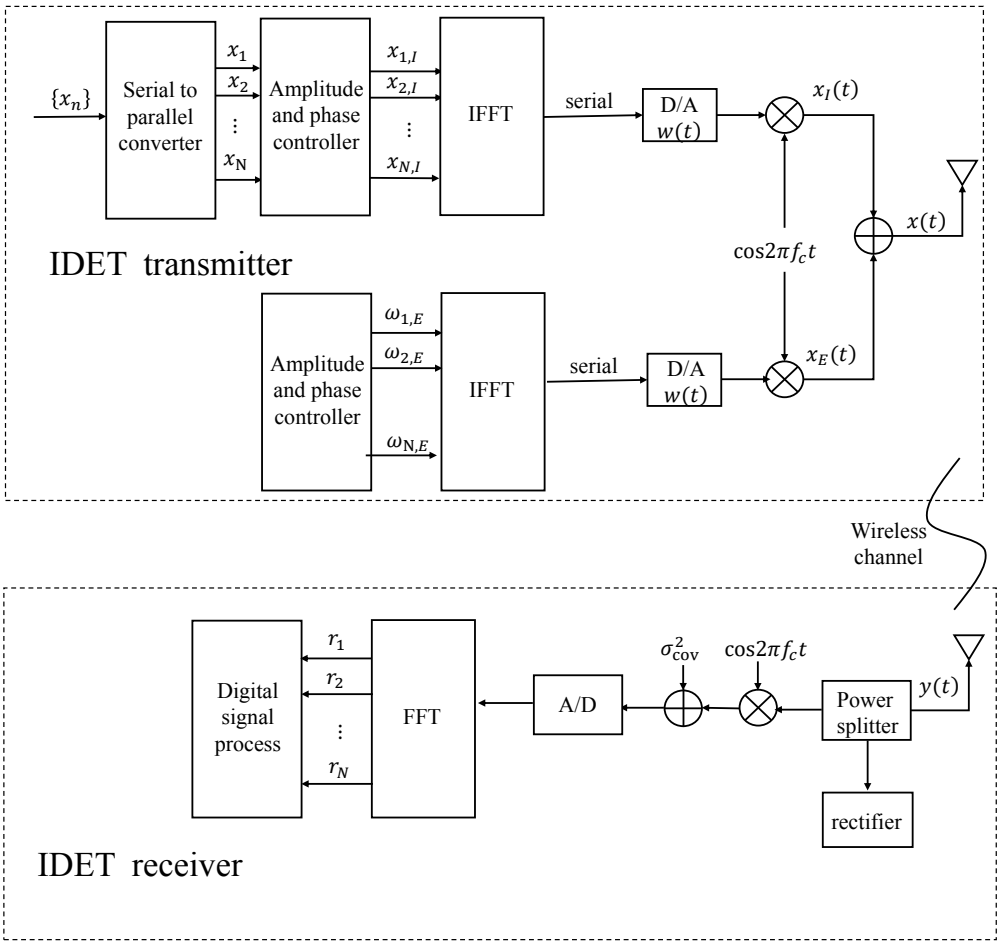

Figure 1. *System transmitter and receiver.*

also impractical for an IoE device with simple hardware and energy shortage. Therefore, employing the outdated CSI to shape the IDET signals is of great significance. Aging channels have been widely used for modelling temporal correlation [27–29]. However, they were never considered in the IDET waveform design.

Against this background, our novel contributions are summarise as follows:

- A practical IDET transceiver is proposed. With the aid of inverse-fast-fourier-transformation (IFFT), the IDET transmitter is capable of generating superposition IDET waveforms with arbitrary amplitudes and phases in the digital domain. The IDET receiver can also adjust its power splitter to balance the WDT and WET performance.
- The carrier asyncrhonisation, due to the hardware limitations and the movements, is assumed between the IDET transmitter and receiver. The resultant CFO induces the inter-subcarrier interference, which degrades the IDET performance. Our waveform design is capable of overcoming the adverse effect of the CFO.
- By exploiting the temporal correlation of aging channels, our waveform design only requires the CSI of the first transmission frame within a block to achieve the maximum IDET performance. This significantly reduces the burden of CSI acquisition on the IDET system.
- The average direct-current harvested by the IDET receiver among all the transmission frames within a block is maximised by jointly designing the amplitudes and phases for every component of multi-sinusoidal WET waveforms and for every subcarrier of OFDM WDT waveforms. Moreover, the power splitter at the IDET receiver is also opti-

mally designed.

- An iterative algorithm is developed by decomposing the original problem into an subproblem of amplitude optimisation and another of phase optimisation. Specifically, the amplitude optimisation is obtained by exploiting a reversed geometric programming method, while the phase optimisation is obtained by an artificial bee colony (ABC) method.

The rest of the paper is organised as below: The system model is introduced in Section II, which is followed by the problem formulation in Section III. After introducing our algorithm for joint amplitude and phase design in Section IV, key simulation results are provided in Section V. Finally, we conclude the paper in Section VI.

Notation: a is a scalar; **a** is a vector; $||\cdot||_2^2$ refers to the norm of a vector; The operation of $\mathbb{E}$ takes the average of the input random variable.

II. SYSTEM MODEL

As portrayed in Figure 1, an IDET transceiver relies upon a superposition waveform constituted by a multi-sinusoidal waveform for WET and an OFDM waveform for WDT. Let us assume that these two kinds of waveforms have N orthogonal components (subcarriers) with frequencies of $\{f_n|n = 1, \cdots, N\}$. We assume that every subcarrier occupies the same bandwidth B and that adjacent subcarriers have a frequency space of Δf. Therefore, the n-th subcarrier has a frequency of $f_n = f_1 + (n-1)\Delta f$. Moreover, the central frequency of the entire IDET waveform is $f_c = (f_1 + f_N)/2$.

2.1 IDET Transmitter

The top box of Figure 1 illustrates a IDET transmitter. We define a transmission block consisting of L transmission frames in total. In the l-th transmission frame, the transmit IDET signal $x(t,l)$ consists of the OFDM based WDT signal $x_I(t,l)$ which carries modulated data symbols $\{x_n(l)|n = 1, \cdots, N\}$ and multi-sinusoidal WET signal $x_E(t,l)$. The n-th symbol can be further expressed as $x_n(l) = s_n(l)e^{j\phi_n(l)}$, which modulates information on its amplitude $s_n(l)$ and phase $\phi_n(l)$. Furthermore, the modulated symbol $x_n(l)$ on the n-th subcarrier obeys a complex Gaussian distribution with zero-mean and a unity variance. In order to counteract the adverse channel fading, the phase and amplitude controller shapes the original modulated symbols in both amplitude- and phase-domains. The resultant shaped symbol on the n-th subcarrier is then expressed as $x_{n,I}(l) = x_n(l)\omega_{n,I}(l) = x_n(l)s_{n,I}(l)e^{j\phi_{n,I}(l)}$, where the complex $\omega_{n,I}(l) = s_{n,I}(l)e^{j\phi_{n,I}(l)}$ represents how we shape the symbol $x_n(l)$ on the n-th subcarrier. By converting the baseband WDT signal to the passband with a central frequency of f_c, the transmit WDT signal during the l-th transmission frame is expressed as:

$$x_I(t,l) = \mathrm{Re}\left[\sum_{n=1}^{N} x_n(l)\omega_{n,I}(l)w(t,l)e^{j2\pi f_n t}\right]. \quad (1)$$

Note that the transmit rectangular window function $w(t,l)$ can be expressed as:

$$w(t,l) = \begin{cases} 1/T, & (l-1)T \le t \le lT, \\ 0, & others, \end{cases} \quad (2)$$

where T is a symbol duration.

Similarly, as shown in the top box of Figure 1, the multi-sinusoidal WET waveforms are also generated by a phase-amplitude controller and subsequent IFFT. We denote baseband WET signals in the l-th transmission frame as $\{\omega_{n,E}(l) = s_{n,E}(l)e^{j\phi_{n,E}(l)}|\forall n = 1, \cdots, N\}$, where the complex $\omega_{n,E}(l) = s_{n,E}(l)e^{j\phi_{n,E}(l)}$ represents how the n-th component (subcarrier) of the multi-sinusoidal waveform is adjusted. Finally, the baseband WET signal is then converted to the passband with a central frequency of f_c. The transmit WET signal during the l-th transmission frame can be finally expressed as:

$$x_E(t,l) = \mathrm{Re}\left[\sum_{n=1}^{N} \omega_{n,E}(l)w(t,l)e^{j2\pi f_n t}\right]. \quad (3)$$

The passband WET signal $x_E(t,l)$ and WDT signal $x_I(t,l)$ are superimposed in the time domain, which

yields the IDET signal $x(t,l)$ expressed as:

$$\begin{aligned} x(t,l) &= x_I(t,l) + x_E(t,l) \\ &= \mathrm{Re}\Bigg[\sum_{n=1}^{N}\Big(s_n(l)s_{n,I}(l)e^{j(\phi_n(l)+\phi_{n,I}(l))} \\ &+ s_{n,E}(l)e^{j(\phi_{n,E}(l))}\Big)\, w(t,l)e^{j2\pi f_n t}\Bigg]. \end{aligned} \tag{4}$$

Therefore, a waveform shaper for L transmission frames can be expressed as $\{\boldsymbol{s}_E, \boldsymbol{s}_I, \boldsymbol{\phi}_I, \boldsymbol{\phi}_E\}$, where all the parameters are $N \times L$ matrices.

2.2 Aging Channel

We assume that the IDET signal propagates through a multipath channel, which has M paths in total. Furthermore, we define $\psi_{n,m}$ as the phase shift in the n-th subcarrier and the m-th signal propagation path, while $a_{n,m}$ represents the corresponding amplitude gain. The channel response in the n-th subcarrier of the m-th path can be denoted as $h_{n,m} = a_{n,m}e^{j\psi_{n,m}}$. Moreover the complex channel response of the n-th subcarrier can be formulated as:

$$h_n = \sum_{m=1}^{M} a_{n,m}e^{j\psi_{n,m}} = a_n e^{j\psi_n}, \tag{5}$$

where we have

$$\begin{aligned} a_n &= \left|\sum_{m=1}^{M} a_{n,m}e^{j\psi_{n,m}}\right|, \\ \psi_n &= \arctan\frac{\mathrm{Im}\left(\sum_{m=1}^{M} a_{n,m}e^{j\psi_{n,m}}\right)}{\mathrm{Re}\left(\sum_{m=1}^{M} a_{n,m}e^{j\psi_{n,m}}\right)}. \end{aligned} \tag{6}$$

In the aging channel, the channel response in the current transmission frame l is temporally correlated to that of the previous frame $(l-1)$. In the n-th subcarrier, the temporal correlation [28] is modelled as:

$$\begin{aligned} h_n(l) &= \alpha h_n(l-1) + \Delta h_n(l) \\ &= \alpha^{l-1}h_n(1) + \sum_{k=1}^{l}\alpha^{l-k}\Delta h_n(k), \end{aligned} \tag{7}$$

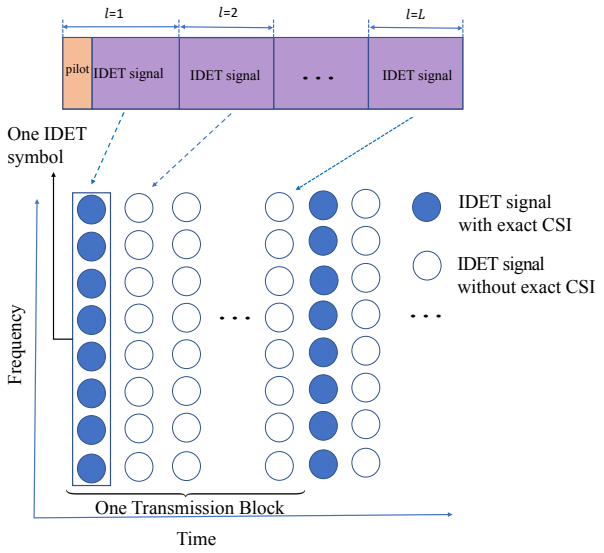

Figure 2. *IDET signal in the time-domain and frequency-domain.*

for $\forall n = 1, \cdots, N$, the correlation factor α satisfies $0 \leq \alpha < 1$. We assume the same correlation factor α for all the subcarriers. Moreover, $\{\Delta h_n(l)|\forall n, l\}$ in Eq. (7) represents the uncertain components, which obeys an independent and identical Gaussian distribution with a zero mean and a variance of $(1-\alpha^2)\sigma_h^2$. Note that σ_h^2 is a common variance for all the channel response $\{h_n(l)|\forall, n = 1, \cdots, N, l = 1, \cdots, L\}$. Moreover, in a specific subcarrier, $\Delta h_n(l)$ is always independent of $h_n(l-1)$.

In order to avoid CSI acquisition for every transmission frame, the outdated CSI can be invoked by the transmitter to generate an appropriate IDET waveform by exploiting the temporal correlation. As shown in Figure 2, we define a transmission block consisting of L transmission frames. The transmitter only needs to acquire the accurate CSI in the very first transmission frame. This CSI is exploited for designing the IDET waveform for the entire block.

2.3 IDET Receiver

The architecture of an IDET receiver is illustrated at the bottom of Figure 1. We denote the CFO between the receiver and the transmitter as Δf_c. With the existence of the CFO, the received passband signal $y(t,l)$ at the l-th transmission frame can be expressed as:

$$y(t,l) = \mathrm{Re}\left[r_I(t,l) + r_E(t,l) + z_a(t)\right], \tag{8}$$

where we have

$$r_I(t,l) = \sum_{n=1}^{N} h_n(l) x_{n,I}(l) \omega_{n,I}(l) \hat{w}(t), \quad (9)$$

$$r_E(t,l) = \sum_{n=1}^{N} h_n(l) \omega_{n,E}(l) \hat{w}(t). \quad (10)$$

Note that $\hat{w}(t) = w(t,l)e^{j2\pi(f_n+\Delta f_c)t}$. To achieve IDET, a power splitter is implemented for splitting $y(t,l)$ into two parts. Note that $\sqrt{\rho(l)}$ of the signal is for energy harvesting. Another portion $\sqrt{1-\rho(l)}$ of the received RF signal is converted to the baseband for the information decoding. The additional noise $z_{cov}(t)$ is imposed by the passband-to-baseband converter on the received signal, which obeys a Gaussian distribution with a zero mean and a variance of σ_{cov}^2. Then, the analog signals pass an analog-to-digital (A/D) converter and a Fast-Fourier-Transformer (FFT) to recover the information carried.

For the receiver, $\{\rho(l)|\forall l = 1,\ldots,L\}$ of power splitter for every transmission frame should be designed to balance the WDT and WET performance.

III. PROBLEM FORMULATION

3.1 WET Performance Analysis

We conceive a Shottky diode based nonlinear energy harvester. After truncating the Taylor series of the diode characteristic equation to the fourth order, the output DC of the l-th transmission frame [30] can be then expressed as:

$$i_{\text{out}}(l) = k_2 \mathbb{E}\left\{\mathcal{P}\left[y_{in}^2(t,l)\right]\right\} + k_4 \mathbb{E}\left\{\mathcal{P}\left[y_{in}^4(t,l)\right]\right\}, \quad (11)$$

where $\mathcal{P}\{\cdot\}$ calculates the time-average of the input stochastic process. It is expressed as:

$$\mathcal{P}[y(t,l)] = \frac{1}{T}\lim_{T\to\infty}\int_0^T y(t,l)dt. \quad (12)$$

Since the noise power of $z_a(t)$ is much lower than that of the superposition IDET signals, its contribution to the output DC is ignored. By substituting Eq. (8) into Eq. (11), we then obtain Eq (13).

$$\begin{aligned} i_{\text{out}}(l) = k_2\rho &\left\{\mathcal{P}\left[r_E^2(t,l)\right] + \mathcal{P}\left[r_I^2(t,l)\right]\right\} \\ &+ k_4\rho^2\left\{\mathcal{P}\left[r_E^4(t,l)\right] + \mathcal{P}\left[r_I^4(t,l)\right]\right. \\ &\left. +6\mathcal{P}\left[r_E^2(t,l)\right]\cdot\mathcal{P}\left[r_I^2(t,l)\right]\right\}. \end{aligned} \quad (13)$$

The detailed expressions of the four terms in Eq. (13), namely $\mathcal{P}[r_E^2(t,l)]$, $\mathcal{P}[r_I^2(t,l)]$,$\mathcal{P}[r_E^4(t,l)]$ and $\mathcal{P}[r_I^4(t,l)]$ can be found in Eq. (14).

In our system, the transmitter does not acquire the accurate CSI until the next channel estimation. As a result, only the outdated CSI is available at the transmitter.

$$\begin{cases} \mathcal{P}\{r_E^2(t,l)\} = \frac{1}{2}\left[\sum_{n=0}^{N-1}|h_n(1)|^2\alpha^{2(l-1)}s_{n,\mathrm{E}}(l)^2 + (1-\alpha^{2(l-1)})s_{n,E}(l)^2\sigma_h^2\right], \\ \mathcal{P}\{r_I^2(t,l)\} = \frac{1}{2}\left[\sum_{n=0}^{N-1}|h_n(1)|^2\alpha^{2(l-1)}s_{n,\mathrm{I}}(l)^2 + (1-\alpha^{2(l-1)})s_{n,\mathrm{I}}(l)^2\sigma_h^2\right], \\ \mathcal{P}\{r_E^4(t,l)\} = \frac{3}{8}\left[\sum_{\substack{n_0,n_1,n_2,n_3 \\ n_0+n_1=n_2+n_3}}\prod_{j=0}^{3}\alpha^{(l-1)}|h_{n_j}(1)|s_{n_j,E}(l)\right] + \frac{3\sigma_h^2}{4}(1-\alpha^{2(l-1)})\left[\sum_{n=0}^{N-1}|s_{n,E}(l)|^2\right]^2, \\ \mathcal{P}\{r_I^4(t,l)\} = \frac{3}{4}\alpha^{4(l-1)}\left[\sum_{n=0}^{N-1}|h_n(1)s_{n,\mathrm{I}}(l)|^2\right]^2 + \frac{3\sigma_h^2}{2}(1-\alpha^{2(l-1)})\left[\sum_{n=0}^{N-1}|s_{n,I}(l)|^2\right]^2. \end{cases} \quad (14)$$

3.2 WDT Performance Analysis

In the received RF signal $y(t,l)$ of Eq. (8), only the WDT signal $r_I(t)$ carries modulated information, while $r_E(t)$ is dedicated for improving the WET performance. After the passband-to-baseband conversion, the received baseband symbol $r_n(l)$ on the n-th sub-carrier during the l-th transmission frame is derived as

$$r_n(l) = \int_{-\infty}^{\infty}\left[r_I(t,l) + r_E(t,l) + \hat{z}(t)\right]e^{-j2\pi f_n t}dt$$

$$= \chi_n \int_{-\infty}^{\infty} w(t,l) e^{j2\pi \Delta f_c t} dt + \widetilde{z} \tag{15}$$
$$+ \sum_{k=1,k\neq n}^{N} \chi_k \int_{-\infty}^{\infty} w(t,l) e^{j2\pi f_n^k t} dt,$$

where we have $\hat{z}(t) = z_a(t) + z_{\text{cov}}(t)$, $\widetilde{z} = \widetilde{z}_a + \widetilde{z}_{\text{cov}}$, $\chi_n = h_n(l)\left(x_{n,I}(l)\omega_{n,I}(l)+\omega_{n,E}(l)\right)$, $\chi_k = h_k(l)\left(x_{k,I}(l)\omega_{k,I}(l)+\omega_{k,E}(l)\right)$, $f_n^k = f_k - f_n + \Delta f_c$. $\widetilde{z}_a$ and $\widetilde{z}_{cov}$ is the projection of the baseband noises. Their variance are σ_a^2 and σ_{cov}^2, respectively. Moreover, let $W(f)$ denote the Fourier transformation of the window function $w(t,l)$. Thus, Eq. (15) can be formulated as:

$$r_n(l) = \chi_n W(\Delta f_c) + \sum_{k=1,k\neq n}^{N} \chi_k W(f_n^k) + \widetilde{z} \tag{16}$$
$$= \alpha_n \frac{\chi_n}{h_n(l)} W(\Delta f_c) + \sum_{k=1,k\neq n}^{N} \alpha_n^k \frac{\chi_k}{h_k(l)} W(f_n^k) + \widetilde{z},$$

where $\alpha_n = \alpha h_n(l-1) + \Delta h_n(l-1)$, $\alpha_n^k = \alpha h_k(l-1) + \Delta h_n(l-1)$. Since $\Delta h_n(l-1)$ is an uncertain component of the CSI, its impact on the IDET performance could be beneficial or detrimental. In the worst case, the term related to $\Delta h_n(l-1)$ is considered as noise or interference. By contrast, in the best case, the term related to $\Delta h_n(l-1)$ can be considered as an additional useful signal to provide extra IDET performance gain [31]. In order to guarantee the lowest WDT performance, we consider a lower-bound of the channel capacity, where the term related to $\Delta h(l-1)$ in Eq. (16) is considered to be noise and interference. Therefore, the lower-bound of the WDT rate during the l-th transmission frame can be expressed as:

$$R_I(l) = \sum_{n=1}^{N} R_n(l) \tag{17}$$
$$= \sum_{n=1}^{N} B\log_2\Bigg(1 + \Big(\frac{(1-\rho(l))(P_{ICI}(l) + P_{I,n,\Delta h}(l))}{(1-\rho(l))\alpha^2 P_{n,I}(l)}$$
$$+ \frac{(1-\rho(l))(P_{E,n,\Delta h}(l) + \sigma_a^2) + \sigma_{cov}^2}{(1-\rho(l))\alpha^2 P_{n,I}(l)}\Big)^{-1}\Bigg).$$

Since the dedicated WET is deterministic, the receiver can obtain the amplitude and the phase of the WET signal. Therefore, the intra-subcarrier-interference imposed by the WET signal can be cancelled. The power $P_{n,I}(l)$ of the desired WDT signal in Eq. (17) can be expressed as:

$$P_{n,I}(l) = \alpha^{2(l-1)} s_{n,I}(l)^2 |h_n(1)|^2 \times |W(\Delta f_c)|^2 \cos^2(\bar{\psi}_{n,I}(l)), \tag{18}$$

where we have $\bar{\psi}_{n,I}(l) = \psi_n(l) + \phi_{n,I}(l)$.While the interference power $P_{n,I,\Delta h}(l)$ and $P_{n,E,\Delta h}(l)$ caused by the outdated CSI during the l-th transmission frame can be expressed as:

$$P_{n,E,\Delta h}(l) = (1-\alpha^{2(l-1)}) s_{n,P}(l)^2 \times \sigma_{\text{h}}^2 |W(\Delta f)|^2 \cos^2(\bar{\psi}_{n,E}(l)), \tag{19}$$
$$P_{n,I,\Delta h}(l) = (1-\alpha^{2(l-1)}) s_{n,I}(l)^2 \times \sigma_{\text{h}}^2 |W(\Delta f)|^2 \cos^2(\bar{\psi}_{n,I}(l)). \tag{20}$$

Similarly, we have $\bar{\psi}_{n,E}(l) = \psi_n(l) + \phi_{n,E}(l)$. Moreover, the power $P_{ICI}(l)$ of the inter-carrier-interference in Eq. (17) is formulated as Eq. (21).

Observe from that both the WET and WDT signal induce the inter-carrier-interference. When the perfect carrier synchronization is achieved, namely $\Delta f_c = 0$, any pairs of subcarriers are totally orthogonal with each other. Otherwise, the resultant inter-carrier-interference cannot be ignored and the system performance can be severely degraded.

$$P_{n,ICI}(l) = E[r_n(l) r_n(l)^*] - P_{n,I}(l) - P_{n,E}(l) - P_{n,E,\Delta h}(l) - P_{n,I,\Delta h}(l)$$
$$= \sum_{k\neq n}^{N} s_{k,I}(l)^2 \left|\alpha^{(l-1)} h_k(1) + \sum_{k=1}^{l} \alpha^{l-k} \Delta h_n(k)\right|^2$$
$$|W(f_k - f_n + \Delta f_c)|^2 + \sum_{\text{k}\neq n}^{N}\sum_{m\neq n}^{N} s_{k,E}(l) s_{m,E}(l)$$
$$|\alpha^{(l-1)} h_k(1) + (1-\alpha^{2(l-1)})\sigma_{\text{h}}^2| \times |\alpha^{(l-1)} h_m(1) + (1-\alpha^{2(l-1)})\sigma_{\text{h}}^2| \times W(f_k - f_n + \Delta f_c)$$
$$W(f_m - f_n + \Delta f_c)\cos(\bar{\psi}_m(l) - \bar{\psi}_k(l)). \tag{21}$$

3.3 Optimization Problem

By acquiring the exact CSI $\boldsymbol{h}(1) = \{h_n(1) = a_n(1)e^{j\psi_n(1)} | \forall n = 1, \cdots, N, \}$ during the first transmission frame of a block having L transmission

frames in total, the IDET signal can be optimally shaped by jointly designing the amplitudes $\boldsymbol{s}_E(l)$ of the WET signal, $\boldsymbol{s}_I(l)$ of the WDT signal, the phases $\boldsymbol{\phi}_E(l)$ of the WET signal, the phases $\boldsymbol{\phi}_I(l)$ of the WDT signal and the power splitting ratio $\rho(l)$ for $\forall l = 1, \cdots, L$. Furthermore, we assume the same transmit power for every transmission frame. We aim to maximise the average output DC for a single transmission block consisting of L transmission frames in total with the maximum transmit power and information rate constraints. As a result, the original optimisation problem (P1) can be reformulated as:

$$\begin{aligned}
(\text{P1}): \max_{\substack{\{\mathbf{s}_I(l),\mathbf{s}_E(l),\boldsymbol{\phi}_I(l),\\ \boldsymbol{\phi}_E(l),\rho(l)|\forall l=1,\ldots,L\}}} \quad & \frac{1}{L}\sum_{l=1}^{l=L} i_{\text{out}}(l) && (22)\\
\text{s.t.} \quad & R_I(l) \geq R_{\min}, \forall l = 1, \cdots, L, && (22a)\\
& \frac{1}{2}\left[||\mathbf{s}_I(l)||_2^2 + ||\mathbf{s}_E(l)||_2^2\right] \leq P,\\
& \forall l = 1, \cdots, L, && (22b)\\
& X_a \rho(l) \in [0,1], \forall l = 1, \cdots, L. && (22c)
\end{aligned}$$

According to Eq. (13) and Eq. (17), $i_{\text{out}}(l)$ and $R_I(l)$ are the functions with respect to variables $\{\mathbf{s}_I(l)$, $\mathbf{s}_E(l)$, $\boldsymbol{\phi}_I(l)$, $\boldsymbol{\phi}_E(l)$, $\rho(l)\}$. Note that (22a)-(22c) constrain the maximum transmit power P, the minimum information rate $R_{\min}$, and the power splitting ratio $\rho(l)$ for every transmission frame, respectively.

IV. JOINT AMPLITUDE AND PHASE DESIGN

4.1 Decoupled Optimisation Problem

Since the transmit power is always the same, (P1) can be equivalently decoupled into L independent sub-problems for maximising the output DC in every transmission frame. Specifically, the l-th sub-problem can be formulated as:

$$\begin{aligned}
(\text{P2}): \max_{\substack{\mathbf{s}_I(l),\mathbf{s}_E(l),\\ \boldsymbol{\phi}_I(l),\boldsymbol{\phi}_E(l),\rho(l)}} \quad & i_{\text{out}}(l) && (23)\\
\text{s.t.} \quad & R_I(l) \geq R_{\min}, && (23a)\\
& \frac{1}{2}\left[||\mathbf{s}_I(l)||_2^2 + ||\mathbf{s}_E(l)||_2^2\right] \leq P, && (23b)\\
& \rho(l) \in [0,1]. && (23c)
\end{aligned}$$

4.2 Amplitudes Optimisation

Given a specific phase design $\{\phi_{n,E}(l), \phi_{n,I}(l)\}$, (P2) is transformed into the following amplitude optimisation problem:

$$\begin{aligned}
(\text{P3}): \max_{\mathbf{s}_I(l),\mathbf{s}_E(l),\rho(l)} \quad & i_{\text{out}}(l) && (24)\\
\text{s.t.} \quad & R_I(l) \geq R_{\min}, && (24a)\\
& (23b)\text{-}(23c),
\end{aligned}$$

where $i_{\text{out}}(l) = i_{\text{out}}(\mathbf{s}_I(l), \mathbf{s}_E(l), \rho(l))$ and $R_I(l) = R_I(\mathbf{s}_I(l), \mathbf{s}_E(l), \rho(l))$. Note that the objective of (P3) is a polynomial function, according to Eq. (13). Therefore, (P3) has a form of Geometric Programming (GP) [32]. By introducing some auxiliary variables, we can transform (P3) into the following equivalent reversed GP problem:

$$\begin{aligned}
(\text{P4}): \max_{\mathbf{s}_E(l),\mathbf{s}_I(l),\rho(l)} \quad & \tau && (25)\\
\text{s.t.} \quad & \tau / \text{i}_{\text{out}}(l) \leq 1, && (25a)\\
& R_{th} \Big/ \left(\prod_{n=0}^{N-1} \gamma_n\right) \leq 1, && (25b)\\
& \frac{\gamma_n}{v_n}\Big[(1-\rho)\left(P_{I,n,\Delta h}(l) + P_{E,n,\Delta h}(l)\right)\\
& \quad + (1-\rho)\left(P_{ICI}(l) + \sigma_a^2\right)\Big] \leq 1,\\
& \quad \forall n = 1, 2 \ldots N, && (25c)\\
& (22b)\text{-}(22c),
\end{aligned}$$

where τ, γ_n and v_n are auxiliary variables. In Eq. (25c), γ_n satisfies $\log_2 \gamma_n \geq \log_2 R_n(l)$, where $R_n(l)$ is the spectral efficiency in the n-th subcarrier in Eq. (17). Moreover, v_n in Eq. (25c) is a function of $\{\mathbf{s}_I(l), \mathbf{s}_E(l), \rho(l)\}$, which is expressed as:

$$\begin{aligned}
v_n(\mathbf{s}_I(l), \mathbf{s}_E(l), \rho(l)) = (1-\rho(l))(P_{n,ICI}(l)\\
+ P_{n,I}(l) + P_{I,n,\Delta h}(l) + P_{E,n,\Delta h}(l)) + \sigma_a^2.
\end{aligned} \quad (26)$$

Note that the inverse of v_n and that of $i_{\text{out}}(l)$ are not polynomials, which prevent the application of GP tools. By employing the classic arithmetic mean and geometric mean (AM-GM) inequality, we approximate a polynomial with a monomial. Specifically, we define that $g_k(\mathbf{s}_E(l), \mathbf{s}_I(l), \rho(l))$ are the monomials in the polynomial $i_{\text{out}}(l) = \sum_{k=1}^{K} g_k(\mathbf{s}_E(l), \mathbf{s}_I(l), \rho(l))$.

Similarly, $g_{n,k}(\mathbf{s}_E(l), \mathbf{s}_I(l), \rho(l))$ represents a monomial term of $v_n(l) = \sum_{k=1}^{K_n} g_{n,k}(\mathbf{s}_E(l), \mathbf{s}_I(l), \rho(l))$. By using AM-GM inequality, we can obtain the following monomials as:

$$\hat{i}_{\text{out}}(l) = \prod_{k=1}^{K} \left(\frac{g_k(\mathbf{s}_E(l), \mathbf{s}_I(l), \rho(l))}{t_k} \right)^{-t_k}, \quad (27)$$

$$\hat{v}_n(l) = \prod_{k=1}^{K_n} \left(\frac{g_{n,k}(\mathbf{s}_E(l), \mathbf{s}_I(l), \rho(l))}{t_{n,k}} \right)^{-t_{n,k}}, \quad \forall n = 1, \ldots, N. \quad (28)$$

where $\hat{i}_{\text{out}}(l)$ and $\hat{v}_n(l)$ are the approximations of $i_{\text{out}}(l)$ and $v_n(l)$, respectively. The value of auxiliary variables $\{t_k, t_{n,k}\}$ should satisfy $\sum_{k=1}^{K} t_k = 1$ and $\{\sum_{k=1}^{K_n} t_{n,k} = 1 | \forall n = 1, \ldots, N\}$. Suppose that we have a set of feasible solution $\{\mathbf{s}_E^{(i)}(l), \mathbf{s}_I^{(i)}(l), \rho^{(i)}(l)\}$ after the i-th iteration. Then, we define $t_k = \frac{g_k(\mathbf{s}_E^{(i)}(l), \mathbf{s}_I^{(i)}(l), \rho^{(i)}(l))}{i_{\text{out}}(\mathbf{s}_E^{(i)}(l), \mathbf{s}_I^{(i)}(l), \rho^{(i)}(l))}$ and $t_{n,k} = \frac{g_{n,k}(\mathbf{s}_E^{(i)}(l), \mathbf{s}_I^{(i)}(l), \rho^{(i)}(l))}{v_n(\mathbf{s}_E^{(i)}(l), \mathbf{s}_I^{(i)}(l), \rho^{(i)}(l))}$. As a result, a standard reversed GP can be formulated as:

$$(\text{P5}): \max_{\mathbf{s_E}(1), \mathbf{s}_I(l), \rho(l)} \quad \tau \quad (29)$$

$$\text{s.t.} \quad \tau \Big/ \hat{\text{i}}_{\text{out}}(l) \leq 1, \quad (29a)$$

$$R_{th} \Big/ \left(\prod_{n=0}^{N-1} \gamma_n \right) \leq 1, \quad (29b)$$

$$\gamma_n \bar{\rho}(l) \left(P_{ICI}(l) + P_{I,n,\Delta h}(l) + P_{E,n,\Delta h}(l) \right) + \gamma_n \sigma_a^2 / \hat{v}_n(l) \leq 1, \quad \forall n = 1, 2, ...N, \quad (29c)$$

(23b)-(23c),

where $\bar{\rho}(l) = 1 - \rho(l)$. Constraints (29a)-(29c) are all transformed into polynomial forms.

A reversed GP aided iterative amplitude design is detailed in Algorithm 1. After initialising variables and calculate the approximated $\hat{i}_{\text{out}}(l)$ and $\hat{v}_n(l)$ of $i_{\text{out}}(l)$ and $v_n(l)$, respectively, as shown in Lines 1-4. (P5) can be effectively solved by an existing optimisation tool, as shown in Line 5 of Algorithm 1 [33]. After sufficient iterations, we may achieve the required accuracy, as shown in Line 8 of Algorithm 1. With the aid of Algorithm 1, we may obtain the amplitude design, when both the phases of the OFDM based WDT signals and those of the multi-sinusoidal WET signals are given.

Ellipsoid method can be invoked to solve a reversed GP problem. Its complexity is $\mathcal{O}((2N)^2)$ [34]. We assume that Δ iterations is required to accurately approximate a polynomial with a monomial. Thus, the complexity of Algorithm 1 is $\mathcal{O}(\Delta(2N)^2)$.

4.3 Phase Optimisation

Given a specific amplitude design $\{\mathbf{s}_E(l), \mathbf{s}_I(l)\}$, the original optimisation problem (P2) is reformulated as:

$$(\text{P6}): \max_{\boldsymbol{\phi}_E(l), \boldsymbol{\phi}_I(l), \rho(l)} \quad i_{\text{out}}(l) \quad (30)$$

$$\text{s.t.} \quad R_I(l) \geq R_{\min}, \quad (30a)$$

(23b)-(23c),

where $i_{\text{out}}(l) = i_{\text{out}}(\boldsymbol{\phi}_E(l), \rho(l))$, and $R_I(l) = R_I(\boldsymbol{\phi}_E(l), \boldsymbol{\phi}_I(l), \rho(l))$. Since the elements of $\boldsymbol{\phi}_E(l)$ and $\boldsymbol{\phi}_I(l)$ are included in trigonometric functions, we invoke an artificial-intelligence based algorithm to find the optimal phase design, namely Artificial Bee Colony (ABC), which is suitable for solving a complex non-convex optimisation problem [35]. Being combined with both local and global searches, an ABC based algorithm imitates the behaviours of bees looking for nectar to find an satisfactory solution, which is detailed in Algorithm 2. The main steps of Algorithm 2 is summarized as below:

- *Step 1*: Randomly generate M feasible solutions as the initial nectar sources in Line 4, where M is the number of nectar sources. Each solution $\boldsymbol{X}_i = \{\boldsymbol{\phi}_E(l), \boldsymbol{\phi}_I(l), \rho(l)\}$ for $\forall i = 1, 2, ..., M$ is a $(2N+1)$-dimension vector representing a single nectar source.

  So we have M different nectar sources in total. Calculate the fitness i_{out} of the i-th solution (the i-th nectar source) in Eq. (13).

- *Step 2*: Both the leader and the follower bees search the nectar sources in Lines 6 and 7. Specifically, every leader bee randomly searches around a specific nectar source (a feasible solution) by obeying the following strategy expressed as:

$$\boldsymbol{X}_i^{j+1} = \boldsymbol{X}_i^j + r\varepsilon(\boldsymbol{X}_i^j - \boldsymbol{X}_k^j), \quad (31)$$

Algorithm 1. *A reverse GP aided algorithm for amplitude design.*

Input: The channel state information $h_n(1)$ of every sub-carriers during the first transmission frame of a block; The required accuracy ϵ;

Output: The amplitudes of information signal $\{\mathbf{s}_E(l)\}$ and the amplitudes of power signal $\{\mathbf{s}_I(l)\}$; The power splitting ratio $\{\rho(l)\}$;

1: Initialise $\mathbf{s}_E(l)$, $\mathbf{s}_I(l)$, $\rho(l)$, $\bar{\rho}(l)$, $i=0$, $i_{\text{out}}^{(0)}=0$;
2: **repeat**
3: Update $i \leftarrow i+1$ and let $\mathbf{s}_E^{(i)}(l)$, $\mathbf{s}_I^{(i)}(l)$, $\rho^{(i)}(l)$, $\bar{\rho}^{(i)}(l) \leftarrow \mathbf{s}_E(l)$, $\mathbf{s}_I(l)$, $\rho(l)$, $\bar{\rho}(l)$
4: Obtain $\hat{v}_n(l) \leftarrow \mathbf{s}_E(l)$, $\mathbf{s}_I(l)$, $\rho(l)$, $\bar{\rho}(l)$ and $\hat{i}_{\text{out}}(l) \leftarrow \mathbf{s}_E^{(i)}(l)$, $\mathbf{s}_I^{(i)}(l)$, $\rho^{(i)}(l)$, $\bar{\rho}^{(i)}(l)$
5: Obtain $\mathbf{s}_E^{(i)}(l)$, $\mathbf{s}_I^{(i)}(l)$, $\rho^{(i)}(l)$, $\bar{\rho}^{(i)}(l)$ by solving (P5) with CVX
6: Let $\mathbf{s}_E(l)$, $\mathbf{s}_I(l)$, $\rho(l)$, $\bar{\rho}(l) \leftarrow \mathbf{s}_E^{(i)}(l)$, $\mathbf{s}_I^{(i)}(l)$, $\rho^{(i)}(l)$, $\bar{\rho}^{(i)}(l)$
7: Let $i_{\text{out}}^{(i)}(l) \leftarrow i_{\text{out}}(\mathbf{s}_E(l), \mathbf{s}_I(l), \rho(l), \bar{\rho}(l))$
8: **until** $|i_{\text{out}}^{(i)}(l) - i_{\text{out}}^{(i-1)}(l)| < \epsilon$

Algorithm 2. *ABC algorithm for phase design.*

Input: The channel state information $h_n(1)$ of every sub-carriers during the first transmission frame of a block; The amplitudes of information signal $\{\mathbf{s}_I(l)\}$ and the amplitudes of power signal $\{\mathbf{s}_E(l) \forall l=1\}$; The size of the transmission block L;

Output: The phases of power signal $\{\boldsymbol{\phi}_E(l)\}$; The phases of information signal $\{\boldsymbol{\phi}_I(l)\}$; The power splitting ratio $\{\rho(l)\}$;

1: Initialise $l=0$, L;
2: **while** $l < L$ **do**
3: Update $l \leftarrow l+1$ and initialise $i=1$
4: Get the M feasible solutions and calculate probability vector $\boldsymbol{P}$ and the fitness vector $\boldsymbol{i}_{\text{out}}$;
5: **while** $i > iter$ **do**
6: The leader bees search and update the nectar sources ;
7: The follower bees search and update the nectar sources;
8: The scout bees search and update the nectar sources;
9: Update the nectar sources;
10: **end while**
11: **end while**

where j represents the j-th iteration, $\varepsilon \in [0,1]$ is a constant, $k \in (1,2,...,M)$ is a random index and different from i, while r is a constant step size. The nectar source is only updated if $\boldsymbol{X}_i^{j+1}$ has a better performance than $\boldsymbol{X}_i^j$. The number of the follower bees is smaller than that of the leader bees. Therefore, we can only assign the follower bees to the nectar sources with a better performance. The probability of a follower bee searching the nectar source $\boldsymbol{X}_i^j$ is obtained as [35]

$$P_i = F_i / \sum_{m=1}^{M} F_i, \tag{32}$$

where $F_i = e^{\frac{i_{\text{out},i}}{\frac{1}{M}\sum_{i=1}^{M} i_{\text{out},i}}}$ is defined as the normalised fitness of this nectar source. Note that a nectar source with a higher normalised fitness has a higher probability to be chosen by a follower bee. Then the follower bee may search around the target nectar source by obeying the same strategy of Eq. (31). The nectar source is only updated, if a better one is found.

- *Step 3*: The scout bees search the nectar sources in Line 8. When the fitness of the nectar source cannot be improved within several iterations, the leader bees give up the original nectar source and they become scout bees searching a new area expressed as:

$$\boldsymbol{X}_i^j = \boldsymbol{X}_{\text{min}}^j + \varepsilon(\boldsymbol{X}_{\text{max}}^j - \boldsymbol{X}_{\text{min}}^j), \tag{33}$$

where $\boldsymbol{X}_{\text{min}}^j$ and $\boldsymbol{X}_{max}^j$ are the lower and upper bound of the $\boldsymbol{X}^j$, respectively.

The cooperation among the leader bees and the follower bees can find a better local solution. Moreover, with the presence of the scout bees, the situation of being trapped in a local optimum can be avoided [36]. Thus, we can obtain a near-optimal solution $\{\boldsymbol{\phi}_E^*(l), \boldsymbol{\phi}_I^*(l), \rho^*(l) | \forall l = 1,\ldots,L\}$, whose fitness is the highest among all the feasible solutions.

4.4 Joint Amplitude and Phase Optimisation

By optimising the amplitudes and phases sequentially, the optimal solutions to every transmission frame are obtained, as shown in Lines 6-11 in Algorithm 3. The original problem (P1) which maximises the average output DC among all the L transmission frames is solved after optimising L sub-problems. The general iterative algorithm for the joint design of both amplitudes and phases for the IDET waveforms is detailed

Algorithm 3. *Joint IDET amplitude and phase waveform.*

Input: The channel state information $h_n(1)$ of every subcarriers during the first transmission frame of a block; The required accuracy ϵ; The size of the transmission block L;

Output: The phases of information signal $\{\boldsymbol{\phi}_I(l)\forall l = 1,\cdots,L\}$; The phases of power signal $\{\boldsymbol{\phi}_E(l)\forall l = 1,\cdots,L\}$; The amplitudes of information signal $\{\boldsymbol{s}_E(l)\forall l = 1,\ldots,L\}$ and the amplitudes of power signal $\{\mathbf{s}_I(l)\forall l = 1,\ldots,L\}$; The power splitting ratio $\{\rho(l)\forall l = 1,\cdots,L\}$;

Initialise $l = 0$, L;
while $l < L$ **do**
  Update $l \leftarrow l + 1$
  Initialise $\mathbf{s}_E(l)$, $\mathbf{s}_I(l)$, $\boldsymbol{\phi}_I(l) = -\boldsymbol{\psi}(1)$, $\boldsymbol{\phi}_E(l) = -\boldsymbol{\psi}(1)$,$\widetilde{i}_{\text{out}} = 0$,$i_{\text{out}} = 0$
  repeat
    Update $\widetilde{i}_{\text{out}} = i_{\text{out}}$
    Obtain $\widetilde{\mathbf{s}}_E(l)$,$\widetilde{\mathbf{s}}_I(l)$ by Algorithm 1
    update $\mathbf{s}_E(l) = \widetilde{\mathbf{s}}_E(l)$, $\mathbf{s}_I(l) = \widetilde{\mathbf{s}}_I(l)$
    obtain $\widetilde{\boldsymbol{\phi}}_E(l)$,$\widetilde{\boldsymbol{\phi}}_I(l)$, $\widetilde{\rho}(l)$ by Algorithm 2
    Update $\boldsymbol{\phi}_E(l) = \widetilde{\boldsymbol{\phi}}_E(l)$, $\boldsymbol{\phi}_I(l) = \widetilde{\boldsymbol{\phi}}_I(l)$, $\rho(l) = \widetilde{\rho}(l)$
    Calculate $i_{\text{out}}(\mathbf{s}_P(l), \mathbf{s}_I(l), \boldsymbol{\phi}_I(l), \boldsymbol{\phi}_E(l), \rho(l))$
  until $|i_{\text{out}} - \widetilde{i}_{\text{out}}| < \epsilon$
end while

in Algorithm 3.

V. SIMULATION RESULTS

For the nonlinear energy harvester, we consider the following parameters: $k_2 = 0.0034$, $k_4 = 0.3859$, and $R_{ant} = 50\ \Omega$, which are in line with [20]. The central frequency is $f_c = 2.4$ GHz and the subcarrier spacing is $\Delta f = 15$ kHz, while $N = 8$ subcarriers are conceived. We define the normalized carrier frequency offset as CFO $= \Delta f_c/\Delta f$. The path-loss from the IDET transmitter to the receiver is modelled as $PL(\text{dB}) = 32.4 + 20\log(d) + 20\log(f_c) + G$, where d is the distance between the IDET transmitter and the receiver [11]. The transmission distance is set to $d = 6.3$ m, the transmit power of the IDET transmitter is $P = 36$ dBm, while the receive antenna gain is $G = 2$ dBi [37]. The small-scale fading of the wireless channel follows the Tapped Delay Line model [38], which models the correlation in the frequency domain.

The channel response during the first transmission frame of a block is portrayed in Figure 3(a), where the correlation in the frequency domain is clearly ob-

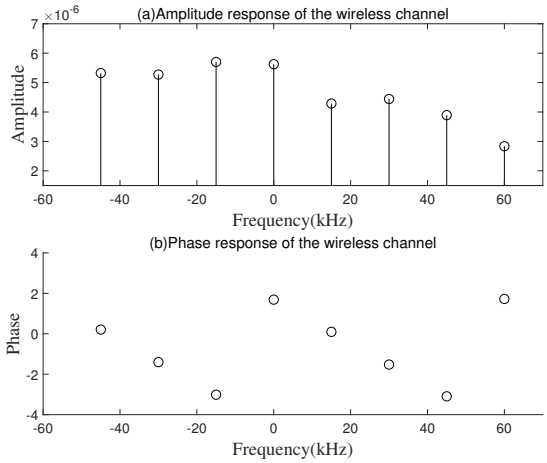

(a) *Wireless channel Rresponse.*

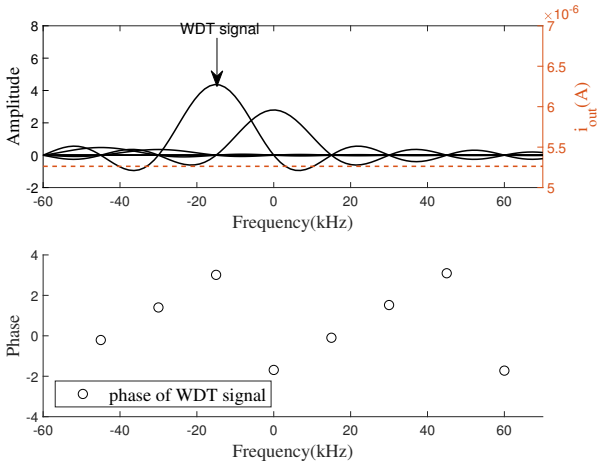

(b) *OFDM waveform shaping.*

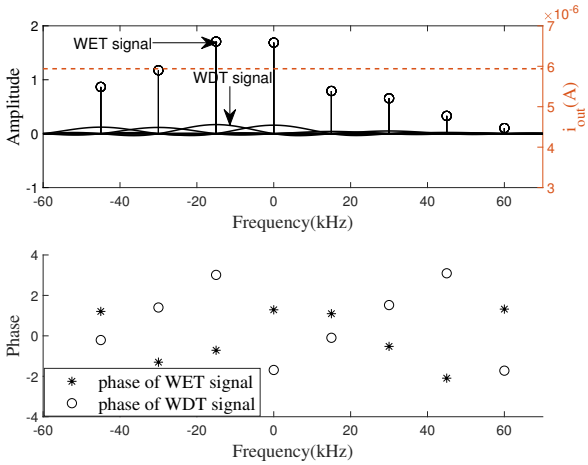

(c) *IDET waveform shaping.*

Figure 3. *An example of waveform design with R_{min} = 1 bps/Hz.*

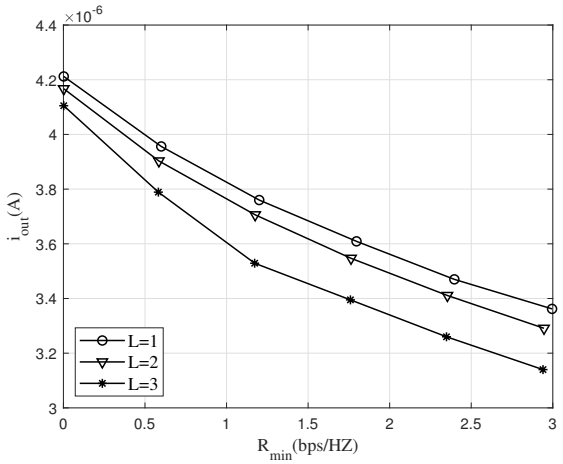

Figure 4. *Output DC with different block size L for $N = 8$, CFO $= 0.025$, $\alpha = 0.97$ and $\sigma_h^2 = 1$ with $B = 15$ kHz.*

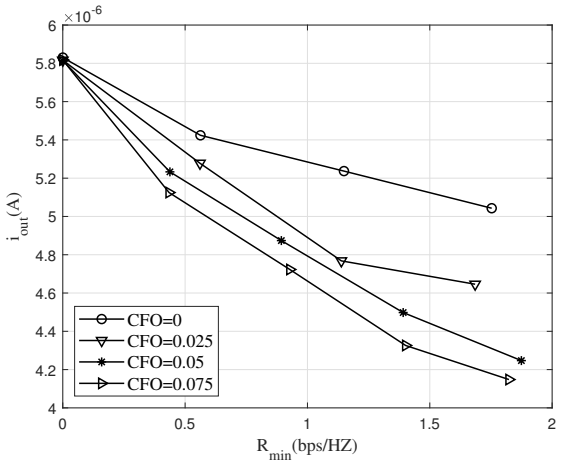

Figure 6. *Output DC with different CFO for $N = 8$, $L = 2$, $\alpha = 0.97$ and $\sigma_h^2 = 1$ with $B = 15$ kHz.*

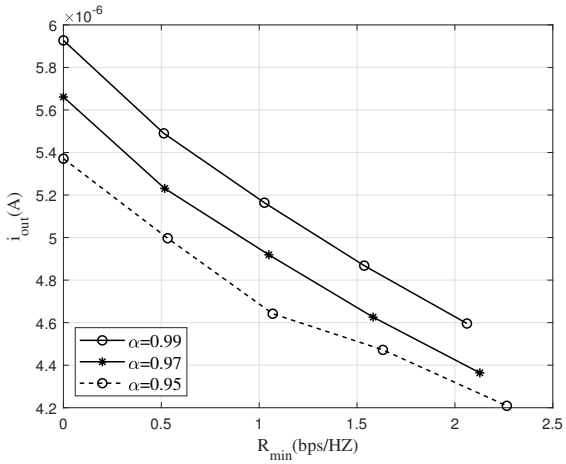

Figure 5. *Output DC with different temporal correlation factor α for $N = 8$, CFO $= 0.025$, $L = 2$ and $\sigma_h^2 = 1$ with $B = 15$ kHz.*

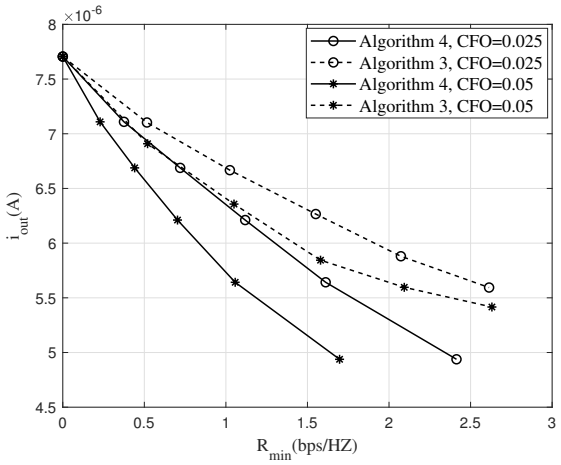

Figure 7. *Algorithm compare for $N = 8$, $\alpha = 0.97$, $L = 2$ and $\sigma_h^2 = 1$ with $B = 15$ kHz.*

served. We illustrate the amplitude and phase design for our IDET waveform and those for the conventional OFDM waveform during this transmission frame in Figure 3(b) and 3(c). Observe from Figure 3(b) that in the OFDM waveform, a single subcarrier associated with the strongest amplitude response gains most of the transmit power in order to maximise the output DC. However, since our IDET waveform is constituted by an OFDM based waveform and a multi-sinusoidal waveform, we can observe from Figure 3(c) that the transmit power is more evenly allocated among all the subcarriers of the OFDM waveform and among all different frequency components of the multi-sinusoidal waveform. Moreover, our simulation results also show that our IDET waveform is capable of achieving the output DC of 5.93×10^{-6} A, while the OFDM waveform only achieves 5.26×10^{-6} A. Note that in this simulation, the WDT requirement is set to 1 bps/Hz.

We investigate the impact of the block size on the IDET performance. We consider 6 transmission frames in total. For $L = 1$, the transmitter may acquire accurate CSI for every transmission frames. For $L = 2$, we have 3 blocks, while we have 2 blocks for $L = 3$. In these two cases, the transmitter only aquires the accurate CSI during the first transmission frame of a block. Observe from Figure 4 that the output DC becomes lower, when the block size increases. This is because the outdated CSI is used for more transmission frames, as L increases. Moreover, the output DC

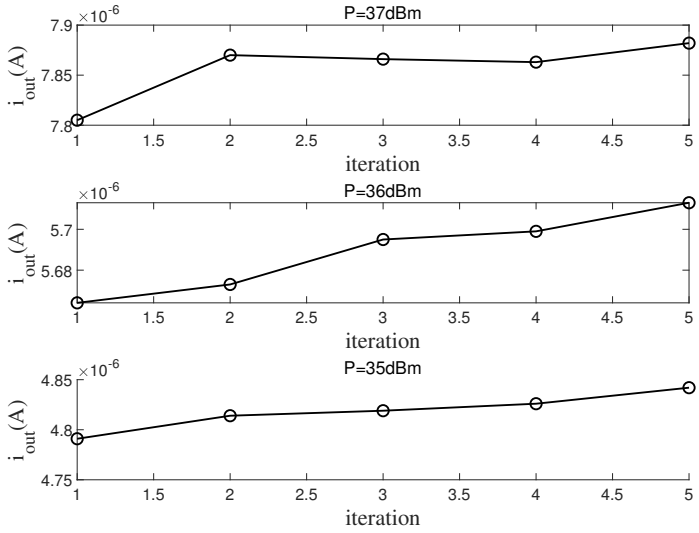

Figure 8. *Convergence performance for Algorithm 3 for* $\alpha = 0.97$ *and* $\delta_h^2 = 1$.

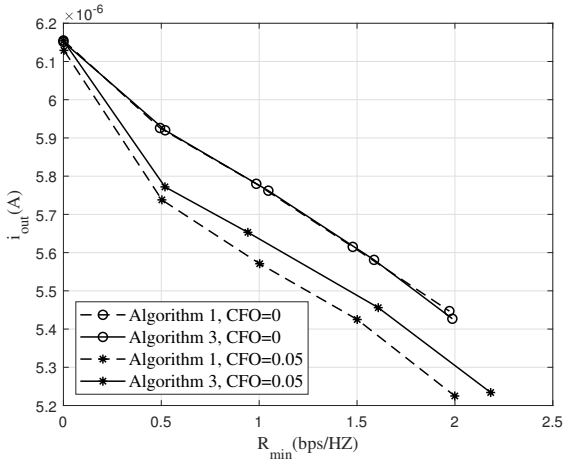

Figure 9. *Algorithm compare for* $N = 8$, $\alpha = 0.97$, $L = 2$ *and* $\sigma_h^2 = 1$ *with* $B = 15$ *kHz.*

also reduces, as the WDT requirement increases. This is because in order to satisfy strict WDT requirement, the transmitter allocates more power to the WDT signal, which thus reduces the WET performance.

We study the impact of the aging channel's temporal correlation factor α on the IDET performance. Observe from Figure 5 that the output DC reduces, as we reduce α. This is because a descreasing α results in a lower temporal correlation of the channel. As a result, the outdated CSI becomes even more inaccurate, which substantially reduces the IDET performance. For example, the average output DC is $i_{\text{out}} = 5.18 \times 10^{-6}$ A as $\alpha = 0.99$. The output DC decreases to $i_{\text{out}} = 4.66 \times 10^{-6}$ A as α reduces to 0.95. Note that the common WDT requirement is set to 1 bps/Hz.

We investigates the impact of the CFO on the IDET performance in Figure 6. Observe from Figure 6 that, the output DC achieves $i_{\text{out}} = 5.16 \times 10^{-6}$ A with CFO $= 0$. However i_{out} degrades to 4.43×10^{-6} A, when the CFO increases to 0.05. Note that the common WDT requirement is set to 1.5 bps/Hz. Since the multi-sinusoidal dedicated WET signal is more efficient than the OFDM based WDT signal in terms of the output DC, the IDET transmitter gradually adapts itself from a pure WET mode by sending multi-sinusoidal WET signals to a pure WDT mode by sending OFDM signals, as the WDT requirement $R_{\min}$ gradually increases from zero to its maximum. The reason is two-fold: 1) The multi-sinusoidal waveform is more efficient than the OFDM waveform for WET. When the WDT requirement is not quite high, the transmitter may allocate more power to the sinusoidal waveform in order to achieve a better output DC. 2) The multi-sinusoidal waveform cannot carry any information. Therefore, when the WDT requirement becomes stricter, the transmitter may reduce the power allocated to the multi-sinusoidal waveform in order to make sure the OFDM waveform satisfy the increasing WDT requirement.

We demonstrate the advantage of our joint design

over the existing scheme, when the CFO is considered. Algorithm 3 is our joint design on the IDET waveform, while Algorithm 4 was proposed in [20] without considering the presence of the CFO and the outdated CSI. Observe from Figure 7 that, when the CFO exists, Algorithm 3 outperforms its counterpart. For example, Algorithm 3 achieves an output DC of $i_{\text{out}} = 6.41\times10^{-6}$ A, while Algorithm 4 only achieves $i_{\text{out}} = 5.62 \times 10^{-6}$ A, when the WDT requirement is 1 bps/Hz and CFO $= 0.05$. As the CFO increases, the performance gain of Algorithm 3 becomes higher.

We study the convergence performance of Algorithm 3 under different transmit power in Figure 8. Observe from Figure 8 that Algorithm 3 has a fast convergence rate, which proves that our optimal design can be solved with a low complexity.

We compare Algorithm 1 and Algorithm 3 under different CFO conditions in Figure 9. Algorithm 1 only optimises the amplitudes of the IDET waveform, while Algorithm 3 optimises both their amplitudes and phases. According to Eq. (21), $\boldsymbol{\phi_E}(l)$ and $\boldsymbol{\phi_I}(l)$ initialised in Line 4 of Algorithm 3 are optimal, when perfect carrier synchronization is conceived. Therefore, there is no difference between two algorithms when CFO $= 0$. When the CFO cannot be ignored, by jointly optimising the amplitudes and phases, Algorithm 3 outperforms its counterpart. For example, the average output DC increases from $i_{\text{out}} = 5.21 \times 10^{-6}$ A to $i_{\text{out}} = 5.3 \times 10^{-6}$ A when CFO $= 0.05$ and the WDT requirement is 2 bps/Hz.

VI. CONCLUSION

By considering the aging channel and the presence of the CFO, we jointly design the amplitudes and phases of the IDET waveforms at the transmitter and the power splitting ratios at the receiver with outdated CSI for maximising the average output DC by considering the presence of the CFO. Our design effectively reduces the control overhead for acquiring accurate CSI for every transmission frame. The original joint design is decoupled into an amplitude design problem and a phase design problem, which can be solved by a reversed GP based algorithm and by an ABC based algorithm, respectively. Then, alternating optimisation is relied upon for obtaining the joint amplitude and phase design. According to the simulation results, we find different waveform design principle for the novel IDET waveform and for the conventional OFDM waveform. Moreover, the performance advantage of our design has been demonstrated by considering the CFO and the outdated CSI.

ACKNOWLEDGEMENT

The authors would like to thank the financial support of Natural Science Foundation of China (No. 61971102, 62132004), MOST Major Research and Development Project (No. 2021YFB2900204), Sichuan Science and Technology Program (No. 2022YFH0022), Key Research and Development Program of Zhejiang Province (No. 2022C01093).

References

[1] J. Hu, Q. Wang, *et al.*, "Energy self-sustainability in full-spectrum 6g," *IEEE Wireless Communications*, vol. 28, no. 1, pp. 104–111, 2021.

[2] W. Wen, Y. Jia, *et al.*, "Joint scheduling and resource allocation for federated learning in SWIPT-enabled micro UAV swarm networks," *China Communications*, vol. 19, no. 1, pp. 119–135, 2022.

[3] J. Hu, K. Yang, *et al.*, "Integrated data and energy communication network: A comprehensive survey," *IEEE Communications Surveys Tutorials*, vol. 20, no. 4, pp. 3169–3219, 2018.

[4] X. Wu, Y. He, *et al.*, "Computation rate maximization in multi-user cooperation-assisted wireless-powered mobile edge computing with ofdma," *China Communications*, vol. 20, no. 1, pp. 218–229, 2023.

[5] Q. Yue, J. Hu, *et al.*, "Transceiver design for simultaneous wireless information and power multicast in multi-user mmwave mimo system," *IEEE Transactions on Vehicular Technology*, vol. 69, no. 10, pp. 11 394–11 407, 2020.

[6] F. Zhu, F. Gao, *et al.*, "Robust simultaneous wireless information and power transfer in beamspace massive mimo," *IEEE Transactions on Wireless Communications*, vol. 18, no. 9, pp. 4199–4212, 2019.

[7] Y. Zhao, J. Hu, *et al.*, "Receive spatial modulation aided simultaneous wireless information and power transfer with finite alphabet," *IEEE Transactions on Wireless Communications*, pp. 1–1, 2020.

[8] C. Pan, H. Ren, *et al.*, "Intelligent reflecting surface aided mimo broadcasting for simultaneous wireless information and power transfer," *IEEE Journal on Selected Areas in Communications*, vol. 38, no. 8, pp. 1719–1734, 2020.

[9] J. Hu, Y. Zhao, *et al.*, "Modulation and coding design for simultaneous wireless information and power transfer," *IEEE Communications Magazine*, vol. 57, no. 5, pp. 124–130, 2019.

[10] Y. Zhao, J. Hu, *et al.*, "Unary coding design for simultaneous wireless information and power transfer with practical m-qam," *IEEE Transactions on Wireless Communications*, vol. 20, no. 5, pp. 2850–2862, 2021.

[11] J. Hu, M. Li, *et al.*, "Unary coding controlled simultaneous wireless information and power transfer," *IEEE Transactions on Wireless Communications*, vol. 19, no. 1, pp. 637–649, 2020.
[12] J. Hu, G. Liang, *et al.*, "Simultaneous wireless information and power transfer with fixed and adaptive modulation," *Digital Communications and Networks*, vol. 8, no. 3, pp. 303–313, 2022.
[13] Y. Zhao, J. Hu, *et al.*, "Joint interleaver and modulation design for multi-user swipt-noma," *IEEE Transactions on Communications*, vol. 67, no. 10, pp. 7288–7301, 2019.
[14] B. Clerckx and E. Bayguzina, "Waveform design for wireless power transfer," *IEEE Transactions on Signal Processing*, vol. 64, no. 23, pp. 6313–6328, 2016.
[15] D. I. Kim, J. H. Moon, *et al.*, "New swipt using papr: How it works," *IEEE Wireless Communications Letters*, vol. 5, no. 6, pp. 672–675, 2016.
[16] I. Krikidis and C. Psomas, "Tone-index multisine modulation for swipt," *IEEE Signal Processing Letters*, vol. 26, no. 8, pp. 1252–1256, 2019.
[17] X. Zhao, Y. Zhang, *et al.*, "Hybrid precoding for an adaptive interference decoding swipt system with full-duplex iot devices," *IEEE Internet of Things Journal*, vol. 7, no. 2, pp. 1164–1177, 2020.
[18] L. Xia, X. Wang, *et al.*, "Signal clipping at transmitter and receiver of O-OFDM for vlc under optical power constraint," *China Communications*, vol. 19, no. 6, pp. 154–168, 2022.
[19] P. Wei, Y. Xiao, *et al.*, "Performance analysis of n-continuous ofdm systems with low-interference signal," *China Communications*, vol. 19, no. 11, pp. 209–230, 2022.
[20] B. Clerckx, "Wireless information and power transfer: Nonlinearity, waveform design, and rate-energy tradeoff," *IEEE Transactions on Signal Processing*, vol. 66, no. 4, pp. 847–862, 2018.
[21] J. Kim, B. Clerckx, *et al.*, "Experimental analysis of harvested energy and throughput trade-off in a realistic swipt system," in *2019 IEEE Wireless Power Transfer Conference (WPTC)*, pp. 1–5, 2019.
[22] R. F. Buckley and R. W. Heath, "System and design for selective ofdm swipt transmission," *IEEE Transactions on Green Communications and Networking*, vol. 5, no. 1, pp. 335–347, 2021.
[23] M. N. Khormuji, B. M. Popović, *et al.*, "Enabling swipt via ofdm-dc," in *2019 IEEE Wireless Communications and Networking Conference (WCNC)*, pp. 1–6, 2019.
[24] D. Xu and H. Zhu, "Outage minimized resource allocation for multiuser ofdm systems with swipt," *IEEE Access*, vol. 7, pp. 79 714–79 725, 2019.
[25] X. Huo, W. Guo, *et al.*, "Analysis and compensation of frequency offset in co-site adjacent channel interference suppression," *China Communications*, pp. 1–13, 2023.
[26] A. Tusha, S. Doğan, *et al.*, "Performance analysis of frequency domain im schemes under cfo and iq imbalance," in *2019 IEEE 30th Annual International Symposium on Personal, Indoor and Mobile Radio Communications (PIMRC)*, pp. 1–5, 2019.
[27] S. Savazzi and U. Spagnolini, "Optimizing training lengths and training intervals in time-varying fading channels," *IEEE Transactions on Signal Processing*, vol. 57, no. 3, pp. 1098–1112, 2009.
[28] C. Chun, J. Kang, *et al.*, "Adaptive rate and energy harvesting interval control based on reinforcement learning for swipt," *IEEE Communications Letters*, vol. 22, no. 12, pp. 2571–2574, 2018.
[29] J. Zheng, J. Zhang, *et al.*, "Impact of channel aging on cell-free massive mimo over spatially correlated channels," *IEEE Transactions on Wireless Communications*, vol. 20, no. 10, pp. 6451–6466, 2021.
[30] B. Clerckx, R. Zhang, *et al.*, "Fundamentals of wireless information and power transfer: From rf energy harvester models to signal and system designs," *IEEE Journal on Selected Areas in Communications*, vol. 37, no. 1, pp. 4–33, 2019.
[31] M. Medard, "The effect upon channel capacity in wireless communications of perfect and imperfect knowledge of the channel," *IEEE Transactions on Information Theory*, vol. 46, no. 3, pp. 933–946, 2000.
[32] S. Boyd, S. J. Kim, *et al.*, "A tutorial on geometric programming," *Optimization & Engineering*, vol. 8, no. 1, p. 67, 2007.
[33] M. Grant, "CVX : Matlab software for disciplined convex programming," http://cvxr.com/cvx/, 2015.
[34] R. G. Bland, D. Goldfarb, *et al.*, "Ellipsoid method: A survey," *Operations Research*, vol. 29, no. 6, pp. 1039–1091, 1981.
[35] L. Zhang, "A gravitational artificial bee colony optimization algorithm and application," in *2018 Eighth International Conference on Instrumentation Measurement, Computer, Communication and Control (IMCCC)*, pp. 1839–1842, 2018.
[36] L. Cheng, M. Yu, *et al.*, "An improved artificial bee colony algorithm based on beetle antennae search," in *2019 Chinese Control Conference (CCC)*, pp. 2312–2316, 2019.
[37] J. Kim, B. Clerckx, *et al.*, "Signal and system design for wireless power transfer: Prototype, experiment and validation," *IEEE Transactions on Wireless Communications*, vol. 19, no. 11, pp. 7453–7469, 2020.
[38] J. Meredith, "Study on channel model for frequency spectrum above 6 ghz," 3GPP TR 38.900, Jun, *Tech. Rep.*, 2016.

Biographies

Jie Hu [S'11, M'16, SM'21] (hujie@uestc.edu.cn) received his B.Eng. and M.Sc. degrees from Beijing University of Posts and Telecommunications, China, in 2008 and 2011, respectively, and received the Ph.D. degree from the School of Electronics and Computer Science, University of Southampton, U.K., in 2015. Since March 2016, he has been working with the School of Information and Communication Engineering, University of Electronic Science and Technology of China (UESTC). He is now a Research Professor and PhD supervisor. He won UESTC's Academic Young Talent Award in 2019. Now he is supported by the "100 Talents"

program of UESTC. He is an editor for *IEEE Wireless Communications Letters*, *IEEE/CIC China Communications* and *IET Smart Cities*. He serves for *IEEE Communications Magazine*, *Frontiers in Communications and Networks* as well as *ZTE Communications* as a guest editor. He is a technical committee member of ZTE Technology. He is a program vice-chair for IEEE TrustCom 2020, a technical program committee (TPC) chair for IEEE UCET 2021 and a program vice-chair for UbiSec 2022. He also serves as a TPC member for several prestigious IEEE conferences, such as IEEE Globecom/ICC/WCSP and etc. He has won the best paper award of IEEE SustainCom 2020 and the best paper award of IEEE MMTC 2021. His current research focuses on wireless communications and resource management for B5G/6G, wireless information and power transfer as well as integrated communication, computing and sensing.

Yaping Hou received the B.Eng. degree from Northwestern Polytechnical University in 2015. And he received the master's degree with the School of Information and Communication Engineering, UESTC in 2022. His research interest includes waveform on simultaneous wireless information and power transfer.

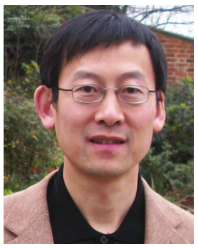

Kun Yang received his Ph.D. from the Department of Electronic & Electrical Engineering of University College London (UCL), UK. He is a Chair Professor in the School of Information and Communication Engineering, UESTC, China. He is also a professor at the School of Computer Science & Electronic Engineering, University of Essex, UK. His main research interests include wireless networks and communications, IoT networking, data and energy integrated networks and mobile computing. He manages research projects funded by various sources. He has published 400+ journal papers and filed 20 patents. He serves on the editorial boards of both IEEE (e.g., *IEEE TNSE, WCL, ComMag*) and non-IEEE journals. He is a Member of Academia Europaca (MAE), IEEE Fellow, IET Fellow.